The Role of Hydrogen Bonding at the Active Site of a Cupredoxin: The Phe114Pro Azurin Variant[†,‡]

Sachiko Yanagisawa, Mark J. Banfield, and Christopher Dennison*

Institute for Cell and Molecular Biosciences, Medical School, University of Newcastle upon Tyne, Newcastle upon Tyne NE2 4HH, United Kingdom

Received April 7, 2006; Revised Manuscript Received May 18, 2006

ABSTRACT: The Phe114Pro mutation to the cupredoxin azurin (AZ) leads to a number of structural changes at the active site attributed to deletion of one of the hydrogen bonds to the Cys112 ligand, removal of the bulky phenyl group from the hydrophobic patch of the protein, and steric interactions made by the introduced Pro. The remaining hydrogen bond between the coordinating thiolate and the backbone amide of Asn47 is strengthened. At the type-1 copper site, the Cu^{II}−O(Gly45) axial interaction decreases, while the metal moves out of the plane formed by the equatorial His46, Cys112, and His117 ligands, shortening the bond to the axially coordinating Met121. The resulting distorted tetrahedral geometry is distinct from the trigonal bipyramidal arrangement in the wild-type (WT) protein. The unique position of the main S(Cys) → Cu^{II} ligand-to-metal charge-transfer transition in AZ (628 nm) has shifted in the Phe114Pro variant to a value that is more typical for cupredoxins (599 nm). This probably occurs because of the removal of the Phe114−Cys112 hydrogen bond. The Phe114Pro mutation results in a 90 mV decrease in the reduction potential of AZ, and removal of the second hydrogen bond to the Cys ligand seems to be the major cause of this change. The C-terminal His117 ligand does not protonate in the reduced Phe114Pro AZ variant, which suggests that none of the structural features altered by the mutation are responsible for the absence of this effect in the WT protein. Upon reduction, the copper displaces further from the equatorial ligand plane and the Cu−S(Met121) bond length decreases. These changes are larger than those seen in the WT protein and contribute to the order of magnitude decrease in the intrinsic electron-transfer capabilities of the Phe114Pro variant.

Cupredoxins are a well-studied class of electron-transfer (ET)[1] proteins that possess a mononuclear type-1 (T1) copper site at which the metal is coordinated by two His ligands and a Cys (*1*−*3*). The metal ion is usually displaced from the plane of these three equatorial ligands in the direction of a weak axially interacting Met, giving a distorted tetrahedral T1 copper-site geometry. In certain cupredoxins (the stellacyanins), a stronger axial interaction with a Gln is present (*4*), and in some T1 copper sites, this ligand is absent [for example, in the plantacyanin from lily (*5*) and the T1 sites of fungal laccases (*6*), ceruloplasmin (*7*), and Fet3p (*8*)]. Azurin (AZ) is unusual among the cupredoxins in that it has two weak axial interactions at its copper site, with Met121 and the backbone carbonyl oxygen of Gly45 resulting in a trigonal bipyramidal arrangement (the equatorial ligands are His46, Cys112, and His117 in AZ) (*9*−*12*). Numerous mutagenesis studies have been devoted to investigating the role of the coordinating residues in cupredoxins (mainly AZ) and have demonstrated that the Cys is the only essential ligand for a site with T1 properties (*13*−*17*). Noncoordinating residues are also important for the structure and function of cupredoxins. The rigid β-barrel scaffold is thought to be essential for constraining T1 copper sites in an arrangement

[†] Financial support for this work was from Universities U.K. (an ORS award to S.Y.) and the University of Newcastle upon Tyne. M.J.B. is supported by a Royal Society (U.K.) University Research Fellowship.

[‡] The coordinates and structure factors have been submitted to the Protein Data Bank (PDB) with codes 2GHZ [Cu^{II} Phe114Pro AZ] and 2GI0 [Cu^{I} Phe114Pro AZ].

* To whom correspondence should be addressed: Institute for Cell and Molecular Biosciences, Medical School, University of Newcastle upon Tyne, Newcastle upon Tyne NE2 4HH, U.K. Telephone: +44-191-222-7127. Fax: +44-191-222-7424. E-mail: christopher.dennison@ncl.ac.uk.

[1] Abbreviations: ET, electron transfer; T1, type 1; AZ, azurin; HOMO, highest occupied molecular orbital; PC, plastocyanin; PAZ, pseudoazurin; AMI, amicyanin; IPTG, isopropyl-β-D-thiogalactopyranoside; MALDI−TOF MS, matrix-assisted laser desorption ionization time-of-flight mass spectrometry; UV/vis, ultraviolet/visible, ϵ, molar absorption coefficient; EDTA, ethylenediaminetetraacetic acid; Hepes, *N*-(2-hydroxyethyl)piperazine-*N*′-(2-ethanesulfonic acid); DPPH, diphenylpicrylhydrazyl; ESE, electron self-exchange; LMCT, ligand-to-metal charge transfer; EPR, electron paramagnetic resonance; NMR, nuclear magnetic resonance; WEFT, water-suppressed equilibrium Fourier transform; E_m, reduction potential; PEG, poly(ethylene glycol), Mes, 2-(*N*-morpholino)ethanesulfonic acid, Tris, tris(hydroxymethyl)aminomethane; MMT, malic acid, Mes, Tris buffer mix; rmsd, root-mean-square deviation; WT, wild type; LF, ligand field; *A*, hyperfine coupling constant; ppm, parts per million; δ_{obs}, observed chemical shift; δ_{pc}, pseudocontact contribution to δ_{obs}; δ_{Fc}, Fermi-contact (through bond) contribution to δ_{obs}; δ_{dia}, the shift in an analogous diamagnetic system, δ_{iso}, the isotropic shift ($\delta_{obs} - \delta_{dia}$); k_{ese}, ESE rate constant; $T_{2,obs}^{-1}$, the observed transverse relaxation rate; $T_{2,red}^{-1}$, the transverse relaxation rate in the fully reduced protein; [Cu^{II}], concentration of oxidized protein; k_2, slope of plots of $T_{2,obs}^{-1}$ against [Cu^{II}]; *I*, ionic strength; K_a, the association constant for homodimer formation; k_{et}, the rate constant for ET; H_{DA}, electronic coupling matrix element; D, donor; A, acceptor; λ, reorganization energy; λ_i, inner-sphere (ligand) reorganization energy; λ_o, outer-sphere (remainder of the protein and solvent) reorganization energy.

10.1021/bi0606851 CCC: $33.50
Published on Web 06/28/2006

ideally suited to fast ET (an entatic state) (*18*). Furthermore, it has been recognized that residues in the second-coordination sphere of the metal influence the electronic structure (*19*−*23*). However, comparatively, few mutations have been made that focus on these features of cupredoxins.

An important attribute of residues in the second-coordination sphere of metal sites in proteins is their hydrogen-bonding capabilities. Amino acids that form hydrogen bonds with ligating residues are particularly important (*24*, *25*), and at a T1 copper site, the coordinating thiolate sulfur of the Cys ligand always accepts one hydrogen bond usually from the backbone amide of an Asn residue (Asn47 in AZ that is adjacent to the His46 ligand) (*1*), which contributes to the T1 copper-site highest occupied molecular orbital (HOMO) (*21*−*23*). In some cupredoxins, including AZ, a second hydrogen bond to the sulfur ligand is provided by the backbone amide of the residue, two after the coordinating Cys on the C-terminal ligand-containing loop [in AZ, Phe114 is the hydrogen-bond donor (*9*, *10*) and the ligands on the loop are Cys112, His117, and Met121]. The corresponding residue is a Pro in other cupredoxins including plastocyanin (PC) (*26*), pseudoazurin (PAZ) (*27*), and amicyanin (AMI) (*28*). This second hydrogen bond has received some attention (*1*, *9*, *22*, *29*), and mutagenesis studies in PAZ and AMI have endeavored to assess the influence of introducing this interaction (*30*−*33*). We have recently characterized AZ variants in which the C-terminal ligand-containing loop has been replaced with shorter sequences (*34*, *35*). These mutations have a limited effect on the structure of the active site, although removal of the second hydrogen bond to the Cys ligand is only one of a number of changes made. To assess solely the influence of removing the second hydrogen bond to the Cys ligand, the Phe114Pro variant of AZ has been prepared and characterized. These studies highlight the importance of residues in the second-coordination sphere for the structure and functionality of metalloproteins.

MATERIALS AND METHODS

Site-Directed Mutagenesis. Mutagenesis was carried out using the QuikChange site-directed mutagenesis kit. The plasmid pTrcAz [a pTrc99A derivative harboring the gene for *Pseudomonas aeruginosa* AZ including the transit peptide (*34*)] along with the following primers were utilized to bring about the mutation: catgttcttctgcaccccgccgggccactccgcg (forward primer) and cgcggagtggcccggcggggtgcagaagaacatg (reverse primer). DNA sequencing of both strands was used to verify the mutation. The pTrc99A derivative harboring the Phe114Pro AZ gene (pTrcF114P_Az) was used as an expression vector.

Cell Growth, Isolation, and Purification of Phe114Pro AZ. Escherichia coli strain TG1 was transformed with pTrcF114P_Az, and cells were grown in the presence of $Cu(NO_3)_2$ (0.5 mM) for approximately 6 h after induction with isopropyl-β-D-thiogalactopyranoside (IPTG) (0.5 mM). Phe114Pro AZ was isolated and purified using a method described previously (*34*). Fractions that gave a single band on a 15% sodium dodecyl sulfate−polyacrylamide gel electrophoresis (SDS−PAGE) gel had an A_{278}/A_{599} ratio of 1.9. The final yield was ∼18 mg/L of cell culture. The observed molecular weight of Phe114Pro AZ is 13 895 Da [determined by matrix-assisted laser desorption ionization time-of-flight mass spectrometry (MALDI−TOF MS)] compared to a theoretical value of 13 894 Da.

Ultraviolet/Visible (UV/Vis) Spectrophotometry. For UV/vis measurements, the protein was oxidized by adding a sufficient volume of a 20 mM solution of $K_3[Fe(CN)_6]$ and exchanged into 10 mM phosphate buffer at pH 8.0 using ultrafiltration. UV/vis spectra were measured at 25 °C on a Perkin−Elmer λ 35 spectrophotometer.

Determination of the Molar Absorption Coefficient. The molar absorption coefficient (ϵ value) of Cu^{II} Phe114Pro AZ was determined using atomic absorption spectroscopy. The protein was fully oxidized and washed with 0.5 mM ethylenediaminetetraacetic acid (EDTA) to remove adventitiously bound metal. The excess oxidant and EDTA were removed, and the protein was exchanged into 10 mM tris(hydroxymethyl)aminomethane (Tris) at pH 8.0 using ultrafiltration. A UV/vis spectrum was acquired, and the copper concentration was determined with a Thermo Electron Corporation (Cambridge, U.K.) M series atomic absorption spectrometer.

Electron Paramagnetic Resonance (EPR) Spectroscopy. X-band EPR spectra were recorded at −196 °C on a Bruker EMX spectrometer. The protein was fully oxidized and washed with 0.5 mM EDTA as described above. The protein sample (∼2 mM) was in 25 mM *N*-(2-hydroxyethyl)-piperazine-*N*′-(2-ethanesulfonic acid) (Hepes) at pH 7.6 plus 40% glycerol. Diphenylpicrylhydrazyl (DPPH) was used as an external reference, and SIMFONIA (Bruker) was used for spectral simulations.

Sample Preparation for Nuclear Magnetic Resonance (NMR) Studies. For electron self-exchange (ESE) rate constant measurements, the protein was exchanged into 20 mM phosphate buffer (99.9% D_2O) at pH* 8.0 (I = 0.06 M). The concentration of Cu^{II} protein was determined by UV/vis by measuring the absorbance at 599 nm (ϵ = 4300 M^{-1} cm^{-1}). Readings were taken before and after the acquisition of NMR spectra, with an average of the two values used for all subsequent calculations. For paramagnetic ^{1}H NMR experiments, the protein was oxidized and exchanged into 10 mM phosphate in 99.9% D_2O at pH* 8.0 using ultrafiltration.

NMR Spectroscopy. ^{1}H NMR spectra were acquired on a JEOL Lambda 500 spectrometer as described previously (*36*). Paramagnetic ^{1}H NMR spectra of the oxidized protein were acquired using the water-suppressed equilibrium Fourier transform (WEFT) pulse sequence. The ESE rate constant determination (at 40 °C) was carried out using the WEFT sequence on Cu^{I} Phe114Pro AZ containing small amounts of the oxidized protein (2−16%). Spin−spin (T_2) relaxation times were derived from peak widths at half-height using the relationship $\nu_{1/2} = (\pi T_2)^{-1}$.

Electrochemistry. The direct measurement of the reduction potential (E_m) was carried out at ambient temperature (22 ± 1 °C) using an electrochemical setup and approach described previously (*37*). Attempts were made with Phe114Pro AZ to find conditions that yielded a satisfactory response using both a gold and a pyrolytic graphite working electrode and with various modifiers (2-diethylaminoethanethiol, 4,4-dithiodipyridine, 3,3′-dithiodiproprionic acid, and diphenyldisulfide for the gold electrode and poly-L-lysine and a mixture of poly-L-lysine and morpholine for the pyrolytic graphite

Table 1: Crystallographic Data Collection and Refinement Statistics

	Cu^{II} Phe114Pro AZ	Cu^{I} Phe114Pro AZ
data collection[a]		
wavelength (Å)	1.542	1.542
space group	$P2_12_12_1$	$P2_12_12_1$
resolution range (Å)	38.8−1.55 (1.63−1.55)	33.1−1.7 (1.79−1.7)
unit-cell parameters (Å)	$a = 35.35$, $b = 47.81$, $c = 132.52$	$a = 35.39$, $b = 47.86$, $c = 132.55$
number of unique reflections	33 091 (4436)	24 113 (3111)
redundancy	6.9 (4.5)	4.9 (5.2)
$I/\sigma(I)$	27.4 (4.8)	20.3 (4.8)
completeness (%)	98.6 (92.7)	94.1 (85.6)
R_{merge} (%)	4.7 (20.4)	6.5 (28.7)
refinement[a]		
resolution	38.8−1.6 (1.64−1.6)	33.1−1.7 (1.74−1.7)
R_{factor} (%)	14.2 (17.3)	17.8 (29.5)
R_{free} (%)	19.0 (26.0)	22.4 (33.6)
rmsd bond lengths (Å)	0.017	0.018
rmsd bond angles (deg)	1.6	1.53
average *B* factor (protein, Å^2)	17.1	15.9
average *B* factor (ligands, Å^2)	29.3	25.9

[a] Figures in parentheses represent data for the highest resolution shell.

electrode). Modification of the electrode surface was performed as described previously (*37*, *38*).

Crystallization and Structure Analysis. Cu^{II} Phe114Pro AZ was crystallized by the hanging drop vapor diffusion method at 20 °C using 2 μL of protein (10 mg/mL in 5 mM Tris at pH 7.5) mixed with 2 μL of precipitant solution [25% poly(ethylene glycol) (PEG) 1500, 100 mM malic acid, 2-(*N*-morpholino)ethanesulfonic acid (Mes), Tris buffer mix (MMT) at pH 4 (the pH-meter reading for this solution was ~5)]. Prior to being frozen in a nitrogen stream, the crystals were immersed in a cryoprotectant (30% PEG 1500, 100 mM MMT buffer at pH 4 plus 20% glycerol). A crystal of Cu^{II} Phe114Pro AZ was reduced by transferring it into 20 μL of the reservoir buffer containing 10 mM ascorbate. The reduction was considered to be complete when the crystal was completely colorless (typically ~3 h). The reduced crystals were transferred to cryobuffer containing 10 mM ascorbate prior to being frozen. Diffraction data were collected at 100 K on a Rigaku Raxis IV^{++} detector with X-rays from a Micromax-007 generator fitted with Osmic "blue" optics. The Cu^{II} structure was solved by molecular replacement using MolRep [as implemented in CCP4 (*39*)] and the *P. aeruginosa* Cu^{II} AZ structure [PDB entry code 4AZU (*40*)] as a search model. The refined Cu^{II} structure was used as a starting model for refinement of the Cu^{I} structure. Iterative model building [using Coot (*41*)] and refinement [Refmac5, as implemented in CCP4] cycles were used to complete the structures of Cu^{II} and Cu^{I} Phe114Pro AZ. In the final stages of refining the Cu^{II} structure, anisotropic *B* factors were refined and hydrogens were added at riding positions while monitoring both the R_{factor} and R_{free}. Detailed data collection and processing statistics are given in Table 1. LSQMAN (*42*) was used to superimpose structures and determine root-mean-square deviation (rmsd) values for C^{α} atoms.

RESULTS

Spectroscopic Properties of Cu^{II} Phe114Pro AZ. The UV/vis spectrum of Phe114Pro AZ is shown in Figure 1 along with that of the wild-type (WT) protein, and peak positions and ϵ values are listed in Table 2. The main S(Cys) → Cu^{II} LMCT band is shifted from 628 nm ($\epsilon = 5100$ M^{-1} cm^{-1}) in WT AZ to 599 nm ($\epsilon = 4300$ M^{-1} cm^{-1}) in the Phe114Pro variant. The ligand-field (LF) bands in Phe114Pro AZ are centered at ~770 nm and are more intense than in the WT protein. The axial EPR spectra of Phe114Pro and WT AZ are shown in Figure 2, and the parameters are listed in Table 2. The most significant alterations caused by the Phe114Pro

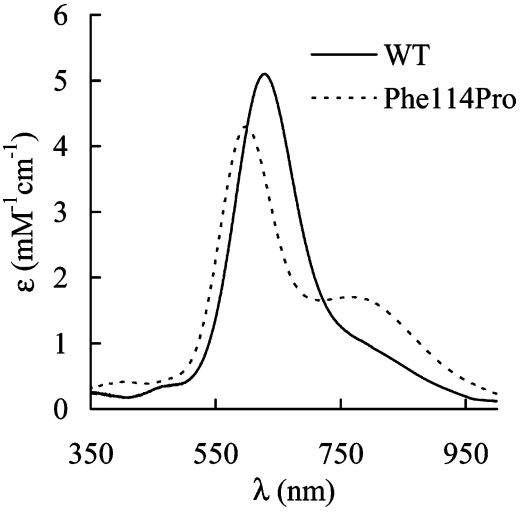

FIGURE 1: UV/vis spectra of Cu^{II} Phe114Pro and WT AZ at 25 °C in 10 mM phosphate at pH 8.0.

Table 2: Properties of Phe114Pro and WT AZ along with the Spectroscopic Features of *Paracoccus versutus* AMI

parameters	Phe114Pro AZ	WT AZ	AMI
UV/vis[a]			
λ_1 (nm) [ϵ_1 (M^{-1} cm^{-1})]	~400 [410]	~460 [360]	~460 [430]
λ_2 (nm) [ϵ_2 (M^{-1} cm^{-1})]	599 [4300]	628 [5100]	596 [3900]
LF transitions centered at (nm) [ϵ (M^{-1} cm^{-1})]	~770 [1700]	~770 [1100]	~765 [1510]
ϵ_1/ϵ_2	0.10	0.07	0.11
EPR[b]			
g_x	2.040	2.035	2.032
g_y	2.046	2.054	2.047
g_z	2.209	2.261	2.235
A_x (mT)	1.3	1.4	0.6
A_y (mT)	1.1	1.4	0.8
A_z (mT)	6.4	5.3	5.4
δ_{obs} Asn47 $C^{\alpha}H$[c]	17.0	19.0	14.1[d]
k_{ese} (M^{-1} s^{-1})[e]	1.4×10^5	2.0×10^6	
E_m (mV)[f]	212	297	
pK_a^{red}	<5[g]	<2[h]	

[a] Measured at 25 °C in 10 mM phosphate pH 8.0. The main band (λ_2) arises from a S(Cys) → Cu^{II} ligand-to-metal charge transfer (LMCT) transition. This band is found at 618 nm ($\epsilon = 4300$ M^{-1} cm^{-1}) in the Phe114Ala AZ variant (*43*). [b] Recorded at −196 °C in 25 mM Hepes at pH 7.6 plus 40% glycerol. All of the EPR parameters were derived from simulations using SIMFONIA (Bruker). The EPR parameters for Phe114Ala AZ are $g_{x,y} = 2.051$, $g_z = 2.246$, and $A_z = 5.3$ mT (*43*). [c] Observed chemical shift [in parts per million (ppm)] measured in 10 mM phosphate at pH* 8.0 (99.9% D_2O) and 25 °C. The corresponding resonance in AMI arises from Asn55. [d] Measured in 50 mM phosphate at pH 7.0 and 32 °C (*44*). [e] Measured in 20 mM phosphate ($I = 0.06$ M) at pH* 8.0 and 40 °C for Phe114Pro AZ and pH* 9.0 for WT AZ (*45*, *46*). [f] Measured in 200 mM Tris at pH 8.1 ($I = 0.20$ M) for Phe114Pro and WT AZ. The E_m value of Phe114Ala AZ is 343 mV in 100 mM KCl plus 10 mM Hepes at pH 8 (*43*). [g] As indicated by the crystallographic and electrochemical studies reported herein. [h] Calculated value for Cu^{I} AZ (*47*).

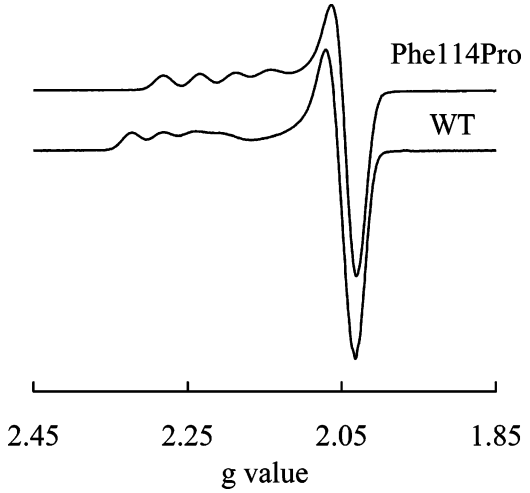

FIGURE 2: EPR spectra of Cu^{II} Phe114Pro and WT AZ at −196 °C in 25 mM Hepes at pH 7.6 (40% glycerol).

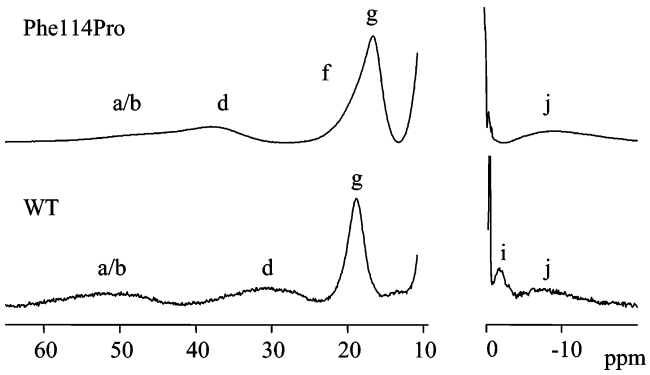

FIGURE 3: ^{1}H NMR spectra (500 MHz) of Cu^{II} Phe114Pro and WT AZ in 10 mM phosphate at pH* 8.0 (99.9% D_2O) at 25 °C (*20*, *34*). The overlapping peaks a and b belong to the $C^{\delta 2}H$ proton resonances of the His ligands. Peak d arises from a $C^{\epsilon 1}H$ resonance of one of the His ligands, and peak g has been assigned to the $C^{\alpha}H$ proton resonance of Asn47. Signal j is the Cys112 $C^{\alpha}H$ proton resonance, while peak f in the spectrum of Phe114Pro AZ, which appears as a shoulder on peak g under these conditions but is resolved at 5 °C, arises from one of the Met121 $C^{\gamma}H$ protons.

mutation are a decrease in the g_z value and a small increase in A_z. Phe114Pro AZ therefore has a classic T1 copper site as does the WT protein (*48*). The paramagnetic ^{1}H NMR spectrum of Cu^{II} Phe114Pro AZ (*20*) is shown in Figure 3, and assignments have been made by a comparison to the data from other cupredoxins (*19*, *20*, *34*−*36*, *44*, *49*). The observed shifts (δ_{obs}) of resonances in these spectra arise from the three contributing factors δ_{dia}, δ_{pc}, and δ_{Fc}, where δ_{dia} is the shift in an analogous diamagnetic system [for example, the Cu^{I} protein], δ_{pc} is the pseudocontact (through space) contribution, and δ_{Fc} is the Fermi-contact (through bond) contribution. The δ_{pc} values are not so significant for Cu^{II} cupredoxins, because of the small anisotropy of the *g* tensor (*19*, *20*, *36*, *44*, *49*), and therefore, δ_{iso} (the isotropic shift, $\delta_{iso} = \delta_{obs} - \delta_{dia}$) for a particular proton provides a good estimate of δ_{Fc}, which is a measure of the spin density. The decreased δ_{obs} for the Asn47 $C^{\alpha}H$ proton resonance indicates a decreased spin density on this residue in the Phe114Pro variant as compared to WT AZ. Signal f, which most likely arises (*19*, *34*−*36*, *44*, *49*) from one of the $C^{\gamma}H$ protons of the axial Met121 ligand in the Phe114Pro variant experiences a sizable δ_{iso}, which is not the case in WT AZ.

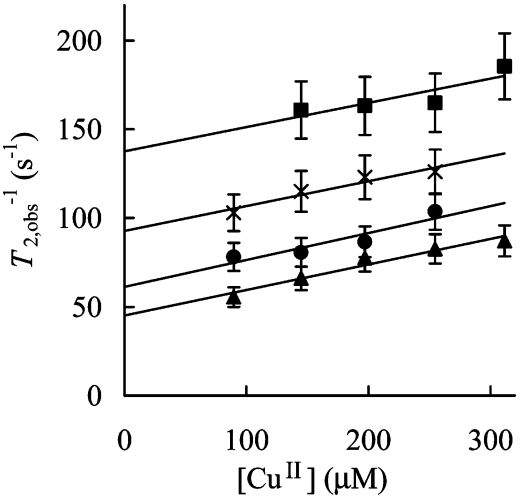

FIGURE 4: Plots (40 °C) of T_2^{-1} against [Cu^{II}] for the signals at 9.7 ppm (■), 7.3 ppm (●), 5.6 ppm (×), and 3.6 ppm (▲) in the WEFT spectrum of Cu^{I} Phe114Pro AZ in 20 mM phosphate buffer (99.9% D_2O) at pH* 8.0.

ESE Rate Constant of Phe114Pro AZ. The ESE rate constant (k_{ese}) of Phe114Pro AZ has been determined at pH* 8.0 by ^{1}H NMR spectroscopy, utilizing the WEFT pulse sequence to select fast relaxing resonances in the Cu^{I} protein in the presence of small amounts of the Cu^{II} form (*36*). Using eq 1

$$T_{2,obs}^{-1} = T_{2,red}^{-1} + k_2[Cu^{II}] \quad (1)$$

where $T_{2,obs}^{-1}$ is the observed transverse relaxation rate of a resonance, $T_{2,red}^{-1}$ is the transverse relaxation rate in the fully reduced protein, [Cu^{II}] is the concentration of oxidized protein, which is valid for protons belonging to the slow-exchange regime, and the rate constant k_2 (the slope of plots of $T_{2,obs}^{-1}$ against [Cu^{II}]) has been determined. Plots of T_2^{-1} against [Cu^{II}] for a number of active-site resonances are shown in Figure 4, yielding k_2 values ranging from 1.4×10^5 to 1.5×10^5 M^{-1} s^{-1}, and a k_{ese} at 40 °C of 1.4×10^5 M^{-1} s^{-1} (average) is obtained for Phe114Pro AZ.

Influence of the Phe114Pro Mutation on the Reduction Potential of AZ. Phe114Pro AZ yields good quasi-reversible responses [anodic and cathodic peaks of equal intensity with separations of ∼60 mV at a scan rate of 20 mV/s and peak currents proportional to the (scan rate)$^{1/2}$ in the range of ∼5−140 mV/s at neutral pH] on a 2-diethylaminoethanethiol-modified gold electrode in 200 mM Tris ($I = 0.20$ M, NaCl) in the pH range of ∼9−6. At pH values below 6, the electrochemical response deteriorates, and by pH 5, reliable cyclic voltammograms cannot be obtained (a wide range of conditions have been investigated, but the signal does not improve). The E_m value of WT AZ was also measured under identical conditions (but mainly using a 4,4-dithiodipyridine-modified gold electrode), and the values obtained are compared in Figure 5. The E_m of Phe114Pro AZ is 212 mV at pH 8.0, which is ∼90 mV lower than that of WT AZ (297 mV). The pH dependence of the E_m of WT AZ in the range studied has been assigned to the protonation of the noncoordinating His35 and His83 (*50*), and an almost identical effect is present in the Phe114Pro variant (the pK_a values for these two His residues are similar in the variant).

Crystal Structure of Cu^{II} Phe114Pro AZ. Phe114Pro AZ crystallizes as a homodimer in which the monomers align

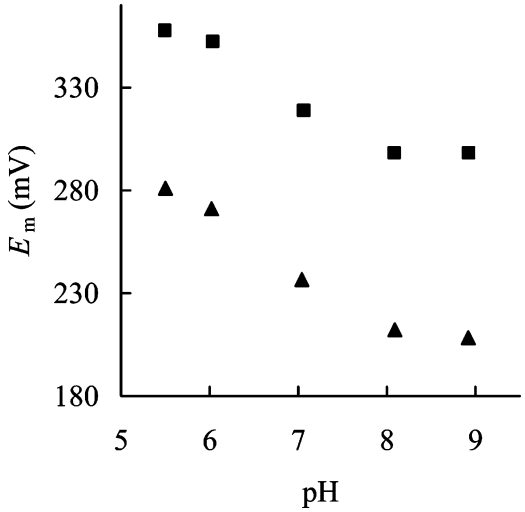

FIGURE 5: Dependence on pH of the E_m of WT (■) and Phe114Pro (▲) AZ in 200 mM Tris ($I = 0.20$ M, NaCl). All of the values are referenced to the NHE at 22 ± 1 °C.

in a parallel fashion with a buried water-accessible surface area of 3500 Å^2. The protein interface contains a number of charged side chains including Lys41, Asp69, Lys70, Asp71, Pro75, Asp76, Lys85, and Glu91. We find no evidence that Phe114Pro AZ forms dimers in solution, which is highlighted by the very similar line widths as in the WT of resonances in the ^{1}H NMR spectrum of the Cu^I forms at high protein concentrations (~2 mM). The packing of molecules in the crystal of Phe114Pro AZ is totally different to that found in the structure of the WT protein in which the monomers associate via the hydrophobic patch that surrounds the exposed His117 ligand (*40*). There are no similar crystal contacts in the structure of Phe114Pro AZ [it is interesting to note that in the structure of the Phe114Ala variant a similar overall arrangement of molecules is found as in the WT crystals (*51*) and is therefore also different from that in the Phe114Pro structure]. It is difficult to say if these packing alterations are due to the mutation made or the different crystallization conditions. The rmsd for all equivalent C$^\alpha$ atoms between the two monomers of Cu^{II} Phe114Pro AZ is 0.18 Å. The overall structure of the Cu^{II} protein is very similar to that of the oxidized WT protein with 126 equivalent C$^\alpha$ atoms that superimpose with rmsd values of 0.52 Å [using 4AZU (*40*) and 1JZF (*11*)]. The eight β strands of Phe114Pro AZ exhibit the highest homology to the WT structure, while the largest backbone changes occur in surface-exposed regions (see Figure 6). In some cases, these alterations can be attributed to the different crystal contacts in the structure of the variant. Three of these changes (in the Pro40−Gly45 loop, the Gly63−Asp69 helix/loop, and the Pro114−His117 region) are in the vicinity of the active site and could result from the Phe114Pro mutation (vide infra). The side chain of Phe114 interacts with the imidazole ring of the His117 ligand in WT AZ and is located on the surface of the protein in the center of the hydrophobic patch, which is important for ET interactions (*53*, *54*). The replacement of Phe114 with a Pro results in the removal of the solvent-exposed phenyl group (see Figure 7A), and the side chain of Tyr72 moves toward the gap created [this side chain moves in a similar manner in loop contraction variants of AZ, vide infra (*35*)], while four water molecules, which are not present in the WT structure, also occupy this space. Three of these waters are >6.5 Å from the copper ion, but one is located only 5.6 Å away and is hydrogen-bonded to the backbone carbonyl oxygen of Gly45 (see Figure 7A). Two of the water molecules more distant from the copper hydrogen bond to the O$^\eta$ of Tyr72 [two waters are also hydrogen-bonded to O$^\eta$ of Tyr72 in the WT structure (*11*, *40*)]. The movement of Tyr72 seems to be linked to a relocation of the backbone in the Gly63−Asp69 region (this includes the end of the α-helical region of AZ) toward the cavity created by the Phe114Pro mutation (see Figure 6). The imidazole ring of His117 moves toward the space vacated by Phe114, and the structure of the protein backbone in the Pro114−His117 region changes slightly (see Figure 6). The N$^{\epsilon 2}$ of His117 is hydrogen-bonded to a water molecule, which bridges with the backbone carbonyl O of Val43 in both WT and Phe114Pro AZ.

A key feature of the Phe114Pro AZ variant is that the second hydrogen bond to the thiolate sulfur of the Cys ligand (donated by the backbone amide of Phe114 in the WT protein) is absent (see Figure 7B). The thiolate sulfur of Cys112 moves by ~1 Å away from the introduced Pro toward the backbone amide of Asn47. The C$^\delta$ of the introduced Pro residue is 3.5 Å from the S$^\gamma$ of Cys112 in Phe114Pro AZ, and it is only 2.6 Å from the position of the S atom in the WT structure (in a superimposition). Therefore, movement of the Cys ligand is partly due to a steric interaction between the thiolate and the introduced Pro as well as being a consequence of enhanced hydrogen bonding of the thiolate with Asn47. The remainder of the active-site hydrogen bonds, in particular those involving residues on the C-terminal ligand-containing loop, are very similar in Phe114Pro and WT AZ (see Table 3).

The lengths of the bonds between the copper and the three equatorial ligands are almost unaltered by the Phe114Pro mutation, although the Cu^{II}−S(Cys112) bond is slightly shorter in the mutant (see Figure 7 and Table 4). The cupric ion is further displaced (by ~0.2 Å) from the plane of the equatorial ligands in the direction of Met121 in Phe114Pro AZ (see Figure 7). This results in a shortening of the Cu^{II}−S(Met121) bond and an increase in the distance between the copper ion and the backbone carbonyl oxygen of Gly45. However, the increase in the Cu^{II}−O(Gly45) distance in the Phe114Pro variant is ~1 Å, which is mainly due to the Gly45 carbonyl oxygen moving away from the metal. Although Phe114 in WT AZ and Pro114 in the mutant are approximately in van der Waals contact with the carbonyl oxygen of Gly45 (~3.3 Å), the altered location of the latter does not seem to be predominantly due to steric effects. The Pro40−Gly45 loop of AZ undergoes a significant shift in the Phe114Pro variant (see Figure 6), compared to a much smaller change observed for the Phe114Ala (*51*) when both are compared to the WT protein. This variation could be due to altered crystal contacts (which are different for each of the proteins). However, the movement of Gly45 could also arise as a consequence of the removal of the hydrogen bond between the residue at position 114 and the Cys112 thiolate. All of these active-site changes give a distorted tetrahedral Cu^{II} geometry in the Phe114Pro AZ variant analogous to those found in cupredoxins, which lack the second hydrogen bond to the Cys (*26*−*28*).

Crystal Structure of Cu^I Phe114Pro AZ. The overall structure of Cu^I Phe114Pro AZ is almost identical to that of

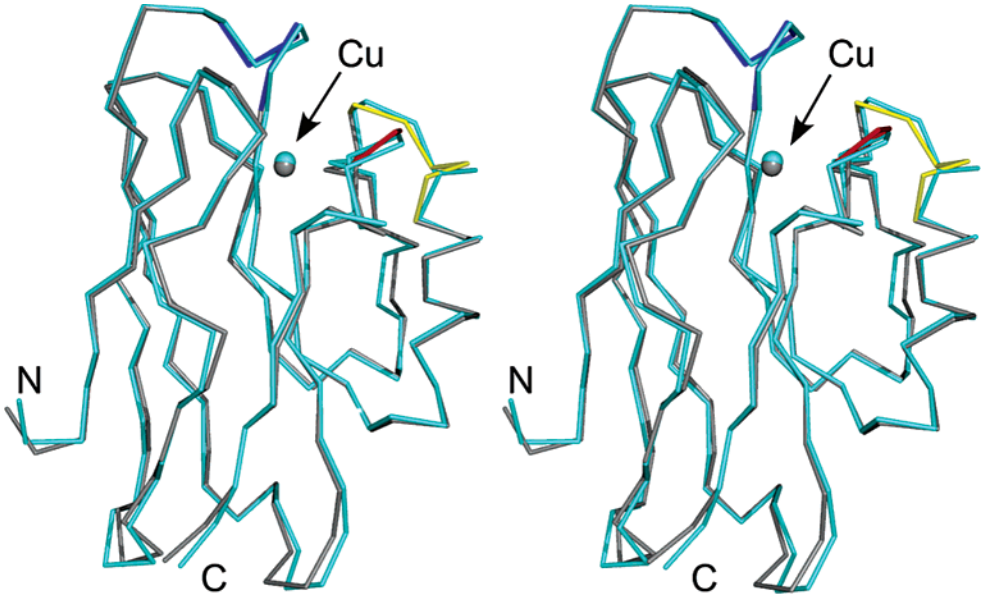

FIGURE 6: Stereoview showing an overlay of the C^{α} traces of Cu^{II} Phe114Pro (gray) and WT (cyan) AZ. For the Phe114Pro variant, residues 40−45, 63−69, and 114−117 are colored blue, yellow, and red, respectively. The Cu^{II} atoms are shown as gray and cyan spheres, and the figure was prepared using PyMol (*52*).

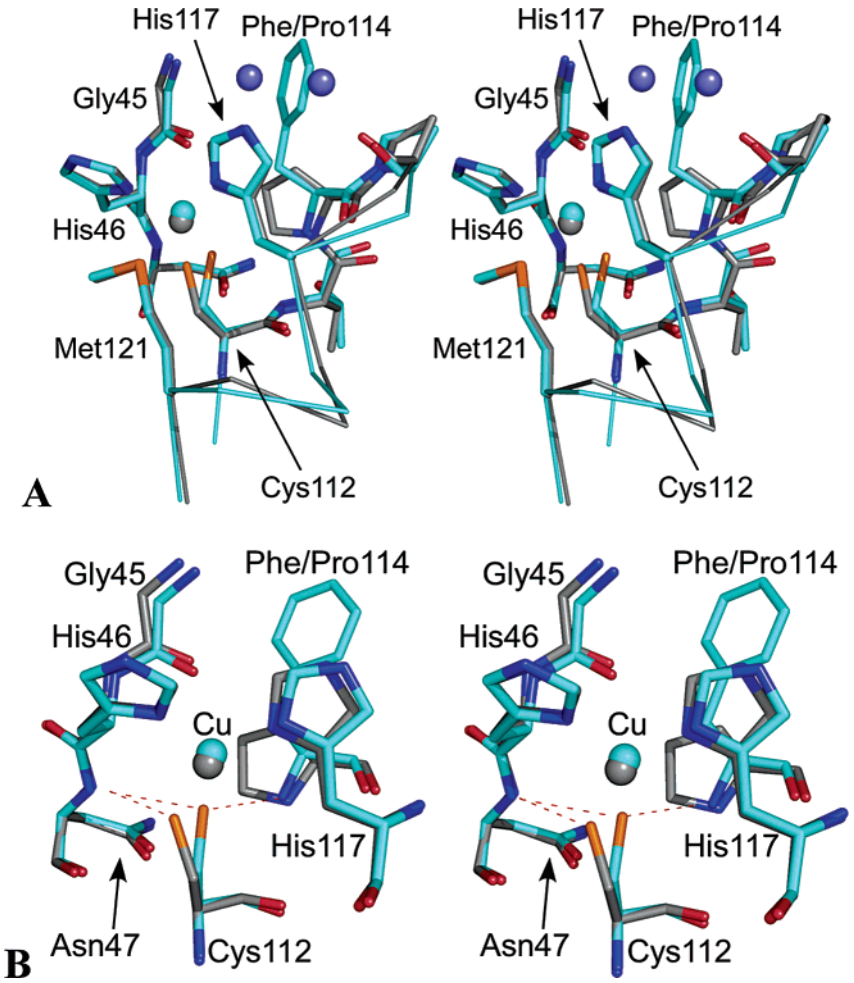

FIGURE 7: Stereoviews showing overlays of the active-site environments in Cu^{II} Phe114Pro (gray) and WT (cyan) AZ prepared using PyMol (*52*). In A, the backbone of residues 111−112 and 116−122 are shown as a C^{α} trace, while all other residues are represented as stick models, and the oxygen atoms of two of the water molecules, which occupy the cavity created by the Phe114Pro mutation, are shown as slate spheres. In B, the altered hydrogen-bonding interactions (dotted red lines) of the Cys112 ligand are highlighted and the movement of His117 as a result of the Phe114Pro mutation is more evident (Met121 has been omitted for clarity).

the Cu^{II} protein, and the C^{α} atoms superimpose with an rmsd of 0.07 Å. At the active site, there are some small alterations (see Figure 8 and Table 4), with two of the three equatorial bonds lengthening as would be expected because of the

Table 3: Hydrogen-Bonding Patterns around the C-Terminal Ligand-Containing Loop of Cu^{II} Phe114Pro and WT AZ

			WT AZ	
atom X	atom Y	Phe114Pro AZ	1JZF[a]	4AZU[b]
Main-Chain−Main-Chain Distances (Å)				
Cys112 N	Met121 O	3.0	3.2	3.2
His117 N	Phe/Pro114 O	2.9	3.0	3.0
Ala119 N	Gly116 O		3.3	3.4[c]
Leu120 N	His117 O	3.1	3.0	3.0
Met121 N	His117 O	2.8	2.7	2.8
Lys122 N	Leu120 O		3.1	3.3
Side-Chain−Main-Chain Distances (Å)				
Cys112 S^{γ}	Asn47 N	3.2	3.6	3.6
Cys112 S^{γ}	Phe114 N		3.4	3.5
Asn47 O^{δ}	Thr113 N	3.0	2.8	2.9[d]
Thr113 O^{γ}	Tyr72 O	2.7	2.7	2.8
Lys122 N^{ζ}	Ala119 O	2.7[e]	4.9	2.9[f]
Side-Chain−Side-Chain Distances (Å)				
Asn47 N^{δ}	Thr113 O^{γ}	3.0	2.9	2.8[d]

[a] Ru^{II}(tpy)(phen)-modified WT AZ from *P. aeruginosa* (*11*). [b] Average from all four chains in the structure of WT AZ from *P. aeruginosa* (*40*). [c] Average of chains B, C, and D. [d] Average of chains A, B, and D. [e] Chain B only. [f] Average of chains A and D.

Table 4: Geometry of the Active Sites of Cu^{II} and Cu^{I} Phe114Pro and WT AZ

	Phe114Pro AZ		WT AZ[a]		WT AZ[b]	
oxidation state	Cu^{II}	Cu^{I}	Cu^{II} (1JZF)	Cu^{I} (1JZG)	Cu^{II} (4AZU)	Cu^{I} (1E5Y)
Cu−Ligand Bond Distances (Å)						
Cu−O (Gly45)	3.60	3.80	2.60	2.67	2.97	3.02
Cu−$N^{\delta 1}$ (His46)	2.09	2.09	2.02	2.06	2.08	2.14
Cu−S^{γ} (Cys112)	2.15	2.25	2.21	2.23	2.24	2.29
Cu−$N^{\delta 1}$ (His117)	1.98	2.02	2.08	2.12	2.01	2.10
Cu−S^{δ} (Met121)	2.92	2.72	3.32	3.31	3.15	3.25
NSN plane[c]	0.24	0.39	0.01	0.05	0.08	0.09
Distance to the Thiolate Sulfur of the Cys Ligand (Å)						
N^{d} (Asn47)	3.2	3.3	3.6	3.5	3.6	3.6
N^{d} (Phe114)			3.4	3.4	3.5	3.4
Angle (deg)						
Gly45−Cu−His46	67	66	80	78	74	75
Gly45−Cu−Cys112	101	99	97	97	99	99
Gly45−Cu−His117	77	72	92	90	89	87
Gly45−Cu−Met121	148	148	150	149	148	145
His46−Cu−Cys112	118	119	132	133	132	133
His46−Cu−His117	101	103	105	105	105	105
His46−Cu−Met121	85	87	72	73	77	73
Cys112−Cu−His117	138	129	123	122	123	122
Cys112−Cu−Met121	107	111	110	111	110	114
His117−Cu−Met121	95	101	85	87	87	88

[a] Ru^{II}(tpy)(phen)-modified WT AZ from *P. aeruginosa* (*11*). [b] WT AZ from *P. aeruginosa* (*40*). [c] The plane containing His46, Cys112, and His117 ligands. [d] Backbone amide nitrogen.

increased ionic radius of reduced copper. The axial interactions differ in the Cu^{I} protein as the cuprous ion displaces further from the His_2Cys plane in the direction of the Met121 ligand. Thus, the Cu−S(Met121) bond length decreases, while the Cu−O(Gly45) distance increases. These active-site changes upon redox interconversion are larger than those observed for the WT protein (see Figure 8 and Table 4).

DISCUSSION

Structural and Spectroscopic Consequences of the Phe114Pro Mutation to AZ. AZ possesses two hydrogen bonds to the sulfur of the coordinating Cys112 (*9*−*12*, *40*). In other cupredoxins such as PC (*26*), PAZ (*27*), and AMI (*28*), only one hydrogen bond to the thiolate group of the corresponding ligand is present. Mutagenesis studies with PAZ and AMI have attempted to introduce a second hydrogen bond to the Cys ligand by replacing Pro80 with Ala and Ile in the former (*30*, *31*) and introducing Ala and Phe in place of Pro94 in the latter (*32*, *33*). Crystal structures of these variants in both the cuprous and cupric forms have been determined (*31*, *33*), and in all cases, it appears, from distances alone, that a hydrogen bond from the backbone amide of the mutated residue to the thiolate sulfur of the Cys ligand has been introduced. However, the observed N−H−S angles of ∼130° in all four variants are not thought to be optimal for hydrogen bonding (the corresponding N−H−S angle is 165° in WT AZ) (*33*). In the case of the Phe114Pro AZ variant, the second hydrogen bond to Cys112 has been removed. This results in a significant increase in the strength of the remaining hydrogen-bonding interaction between Cys112 and the backbone amide of Asn47, which is facilitated by the movement of the thiolate sulfur toward this residue (resulting partly from a steric interaction of the Cys side chain with the introduced Pro). The Cu^{II}−S(Cys112) bond length is significantly shorter in Phe114Pro AZ as compared to the WT protein and is similar to those found in the proteins that do not possess the second hydrogen bond to this ligand (*26*−*28*).

At the Cu^{II} site of Phe114Pro AZ, the metal ion is displaced further from the His_2Cys plane toward the axial Met121 ligand than in the WT protein, which results in a shorter bond to the thioether sulfur, while the copper−O(Gly45) distance increases dramatically, giving a distorted tetrahedral active site analogous to those found in PC (*26*), PAZ (*27*), and AMI (*28*). There are a number of possible reasons for the movement of the carbonyl oxygen of Gly45 away from the copper ion, with the displacement of the Pro40−Gly45 loop as a consequence of altered crystal contacts being the most likely [it should be noted that the copper−O(Gly45) distance differs by ∼0.3 Å in the two available WT AZ structures (see Table 4)]. The movement of Gly45 could also result directly from the removal of the hydrogen bond between the residue at position 114 and the Cys112 thiolate, and thus, these two features of the active site of AZ may be linked. This hydrogen bond is also removed in the loop-contraction mutants in which the C-terminal ligand-containing loop of AZ (C^{112}TFPGH^{117}-SALM^{121}) has been shortened to the corresponding sequence from AMI (C^{112}TPH^{115}PFM^{118}, giving AZAMI) and also in AZAMI-F (C^{112}TPH^{115}PM^{117} loop), and increases in the Cu−O(Gly45) distances, albeit smaller than those seen in the Phe114Pro AZ variant, are observed (*35*). The position of His117 is affected by the Phe114Pro mutation because of the removal of the phenyl ring, which packs against the imidazole moiety of this ligand in WT AZ, and the side chain of Tyr72 moves to partly fill the space created. Water molecules occupy the remainder of this region, and one of these hydrogen bonds to the backbone carbonyl oxygen of Gly45 (not present in WT AZ). An analogous water is found in the structure of AMI (*28*) [and also in a high-resolution structure of PAZ (*27*)] and is not present in the Pro94Phe and Pro94Ala variants. This water is also found in the AZAMI and AZAMI-F loop-contraction variants, which have similar active-site structures as the WT protein (*35*), and thus,

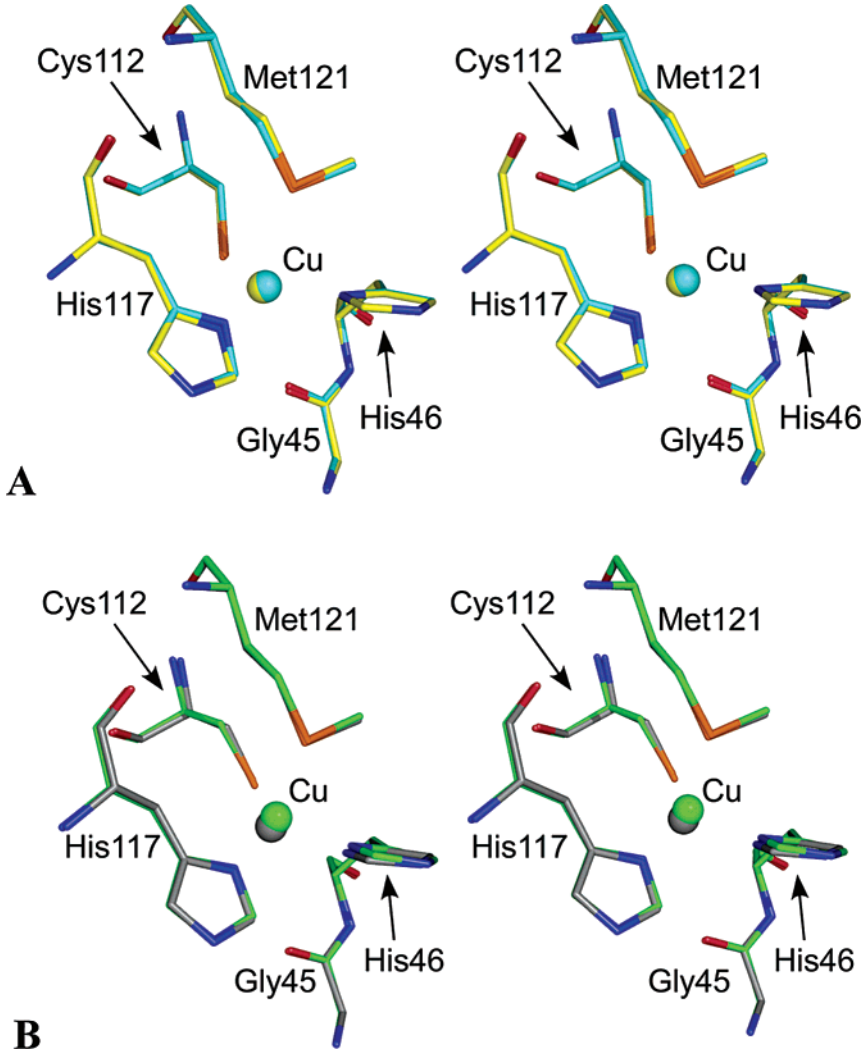

FIGURE 8: Stereoviews showing overlays of (A) the Cu^{II} (cyan) and Cu^{I} (yellow) sites of the WT and (B) the Cu^{II} (gray) and Cu^{I} (green) sites of Phe114Pro AZ prepared using PyMol (*52*).

it appears unlikely that any of the copper-center changes observed in Phe114Pro AZ can be attributed to this water molecule. The space created by the Pro80Ala mutation in PAZ is filled by a water molecule that hydrogen bonds to the backbone carbonyl oxygen of Gly39 but is in a slightly different location (only 4.8 Å from the copper) as that found in the WT protein (*27*) and also in AMI and the AZ variants.

The largest effect of the Phe114Pro mutation on the spectroscopic properties of AZ is the almost 30 nm shift in the position of the main S(Cys) → Cu^{II} LMCT transition, resulting in this band being at a similar wavelength as for almost all other T1 copper sites. The large number of structural changes at the active site of the Phe114Pro variant makes it difficult to identify the exact cause of the unusual position of this band in the WT protein. Whether the second hydrogen bond to the Cys, the orientation of this ligand, or the interaction between the copper and the backbone carbonyl oxygen of Gly45 is responsible cannot be said with any certainty. The hydrogen-bonding network of the Cys112 ligand appears to be the most likely cause as the Pro94Phe mutation in AMI leads to a 12 nm red shift in this band (*32*) and mutations to Asn38 in PC, whose backbone amide hydrogen bonds to the Cys84 ligand, also influence the position of this feature (structures have not been determined for these variants) (*25*). However, other cupredoxins, which possess the second hydrogen bond to the Cys ligand, in particular auracyanin, which exhibits close structural homology to AZ, have their main S(Cys) → Cu^{II} LMCT bands at ~600 nm (*4*, *29*), and the Pro80Ala mutation in PAZ has no effect on the position of this band (*30*). Interestingly, the Phe114Ala and Phe114Val mutations both result in approximately 10 nm shifts to lower wavelength in the position of this band in AZ (*43*), and therefore, the presence of a phenyl group adjacent to His117 may also be important.

The larger δ_{iso} value for the observed $C^{\gamma}H$ proton resonance from Met121 indicates a greater spin density on this ligand, consistent with the increased axial interaction upon making the Phe114Pro mutation. The slightly increased A_z value in the EPR spectrum of Phe114Pro AZ points to a small enhancement of the spin density on the copper. The shorter Cu^{II}−S(Cys112) bond in Phe114Pro AZ along with the removal of one of the two hydrogen bonds to the coordinated thiolate should increase the spin density on the Cys ligand (*23*). This increase and the shorter hydrogen bond between the ligating sulfur of Cys112 and the backbone amide of Asn47 would be expected to increase the spin density on Asn47. However, the decreased δ_{obs} for the Asn47 $C^{\alpha}H$ proton resonance indicates less spin density on this residue. The lower g_z value for Phe114Pro AZ most likely

arises from the decreased interaction with the backbone carbonyl oxygen of Gly45.

Reduction Potential. The decrease in the E_m of AZ upon making the Phe114Pro mutation indicates that the active-site environment of the variant stabilizes Cu^{II} over Cu^{I}. The Pro80Ala and Pro80Ile PAZ mutations give rise to 139 and 180 mV increases in E_m, respectively (*30*, *31*), while the Pro94Ala and Pro94Phe AMI variants have E_m values 115 and 150 mV higher than that of the WT protein, and thus, these mutations all favor the cuprous form (*32*, *33*). The influence of the additional dipole from the water molecule, which occupies the space created by the Pro80Ala mutation in PAZ, on the solvation energy of the copper site has been identified as the main reason for the increased E_m in this variant [the water hydrogen bonded to the backbone carbonyl oxygen of Gly39 in the high-resolution structure of the WT protein (*27*) was not considered when analyzing the effect of this mutation on E_m (*31*)]. The influence of the Pro80Ile mutation on E_m has been attributed to the more trigonal site in the Cu^{I} form than in the WT protein (a similar effect may also be relevant for the Pro80Ala variant). For the Pro94Ala and Pro94Phe AMI variants, it has been suggested that the introduced interaction between the backbone amide of the mutated residue and the Cys ligand removes electron density from the thiolate, which preferentially stabilizes Cu^{I} over Cu^{II} and leads to the observed increase in E_m [this effect can be rationalized electrostatically, whereby the N−H dipole destabilizes Cu^{II}] (*55*, *56*). The consequence of the removal of a water molecule 5.5 Å from the copper, which hydrogen bonds to the backbone carbonyl of Pro52, on the E_m of AMI, has not been considered.

The influence of the Phe114Pro mutation on the E_m of AZ is due to a combination of effects. The removal of the second hydrogen bond to the Cys112 ligand will stabilize the Cu^{II} form and lower E_m (this will be partly offset by the increased hydrogen-bonding interaction with the NH of Asn47) (*55*, *56*). The substantial lengthening of the distance between the copper and the backbone carbonyl oxygen of Gly45 should result in an increase in E_m (*55*). The inclusion of a water molecule hydrogen bonded to the backbone carbonyl oxygen of Gly45 would be expected to decrease E_m, but the effect is probably relatively small given the distance from the copper (5.5 Å). The Phe114Ala mutation leads to a 50 mV increase in the E_m of AZ, which indicates the sizable influence of phenyl group removal alone (*43*, *51*). The altered active-site structure in Phe114Pro AZ must also contribute to the influence of this mutation on E_m. The geometry changes upon reduction compared to WT AZ probably destabilize the Cu^{I} form (*31*), whereas the different strengths of the interactions with the axial ligand should have the opposite effect. Deletion of the hydrogen bond seems to be the dominant effect of the Phe114Pro mutation on the E_m of AZ. Therefore, the number and strength of the hydrogen bonds to the coordinated Cys are a key mechanism for regulating the E_m value of cupredoxins as is also the case for Fe−S clusters in proteins (*55*−*57*).

C-Terminal His Ligand Protonation. The C-terminal His ligand protonates and dissociates from the cuprous ion in certain cupredoxins, with pK_a values ranging from ∼7 to 5 (*3*, *58*−*60*). This effect has a dramatic influence on both E_m (*38*) and the intrinsic ET reactivity (*36*) and is dependent upon kinetic and thermodynamic factors (*38*, *61*). The His95 ligand has a pK_a of 7.5 in Cu^{I} WT AMI (*60*), and values of 6.3 and <5 have been found for the Pro94Ala and Pro94Phe variants, respectively (*32*). The crystal structures of these variants have been determined at pH ∼5.5, and thus, for the Cu^{I} form of Pro94Ala AMI, dissociation of the His95 ligand is observed as in the WT protein (*33*). It has been suggested that the residue at position 94 sterically hinders His95 rotation, which is responsible for the observed effects of the mutations on the pK_a of this ligand (*33*). The His117 ligand does not protonate in the Cu^{I} form of Phe114Pro AZ in the accessible pH range, which is also the case for the Cu^{I} WT protein for which a pK_a value of <2 has been calculated (*47*). In AZ, the distance between the $N^{\delta 1}$ of His117 and the C^{β} of Phe114 is too large to prevent the rotation of His117 (upon protonation). The distance to the side chain of Pro114 in the variant is even greater. The hydrogen-bonding pattern around the active site of AZ and in particular the presence of two hydrogen bonds to the thiolate sulfur of the Cys112 ligand has been suggested as a reason for the absence of His ligand protonation in this cupredoxin (*29*, *62*). This is consistent with the Pro94 mutations in AMI lowering the pK_a of His95 but cannot explain the difference between the Phe and Ala variants (a steric argument has been used to rationalize this effect, vide supra). Furthermore, packing of the imidazole moiety of His117 between the phenyl group of Phe114 and the thioether group of Met13 has also been identified as a possible reason for the absence of His ligand protonation in AZ (*63*). The Phe114Pro mutation removes both the hydrogen bond and the phenyl group, and the His117 ligand does not show any sign of protonating and dissociating in our experiments (it could be that the pK_a value is higher than in WT AZ but occurs at too low a pH value to be observed in the studies that we have performed). His117 does protonate in Cu^{I} AZAMI and AZAMI-F, in which the second hydrogen bond to the Cys ligand and also Phe114 are missing but in which the C-terminal ligand-containing loop has been shortened (*35*). Furthermore, the pK_a value is usually dependent upon the length and sequence of the ligand-containing loop (*3*, *34*, *35*, *64*−*67*), and it therefore appears that this is a key feature of a T1 copper site in controlling His ligand protonation. It has been suggested (*67*) that the effect of loop length is entropic in origin, and studies are currently underway to further investigate this.

ESE Rate Constant. The ET reactivity of Phe114Pro AZ has been assessed by determining its k_{ese} value, which is not influenced by alterations in E_m, because this reaction has no driving force. The k_{ese} is an order of magnitude smaller than that of the WT protein (*45*, *46*), and thus, the Phe114Pro mutation has lowered the ET capability of AZ. ESE is activation-controlled (*68*), and thus, $k_{ese} = K_a k_{et}$, where K_a is the association constant for homodimer formation and k_{et} is the rate constant for ET. ESE in AZ has been shown to involve the association of two molecules via the hydrophobic patch surrounding the exposed His ligand (*53*, *54*), and removal of the phenyl ring from this region in the Phe114Pro variant could decrease K_a. The k_{et} value for ESE depends upon the electronic coupling matrix element (H_{DA}), which is influenced by the donor (D)−acceptor (A) distance and the reorganization energy [λ, which is made up of inner-sphere (ligand, λ_i) and outer-sphere (remainder of the protein and solvent, λ_o) components]. The removal of the bulky

phenyl group in the Phe114Pro variant may influence the distance between the active sites of the two molecules in the homodimer and thus affect k_{et}. The larger structural changes upon reduction in Phe114Pro AZ must also influence ET, by increasing λ_i and contributing to the lower k_{ese} (the enhanced solvent accessibility could alter λ_o). Thus, in AZ, which possesses two axially interacting ligands, two hydrogen bonds to the thiolate sulfur of the coordinating Cys help to keep the copper atom in the equatorial ligand plane upon reduction. Deletion of one of these hydrogen bonds removes constraints from the active site allowing the movement of the copper, on the basis of its hard−soft acid−base preferences, upon redox interconversion, resulting in a less entatic site.

CONCLUSIONS

The Phe114Pro mutation removes a key hydrogen bond, resulting in a number of structural changes at the active site of AZ. All of these alterations influence the E_m value, but the different hydrogen-bonding pattern seems to be dominant. This also appears to be the case if the influence of the Phe114Pro mutation on the spectroscopic properties of AZ is considered. This hydrogen-bonding network does not seem to be a major factor in controlling the ability of the C-terminal His ligand to protonate and dissociate from the Cu^I site of cupredoxins. The modest decrease in ET reactivity of the Phe114Pro variant is partly due to an increased λ value, with diminished homodimer formation probably also contributing. Interestingly, loop-contraction mutations in AZ in which the second hydrogen bond has also been removed have a much less significant effect on the spectroscopy and structure of the Cu^{II} protein. Thus, loop mutations, which make a number of changes to the second-coordination sphere, seem to be more readily accommodated at the active site of a cupredoxin than the individual substitution of key, noncoordinating amino acids.

ACKNOWLEDGMENT

We thank Dr. Chan Li for performing atomic absorption experiments.

REFERENCES

1. Adman, E. T. (1991) Copper protein structures, *Adv. Protein Chem. 42*, 145−197.
2. Nersissian, A. M., and Shipp, E. L. (2002) Blue copper-binding domains, *Adv. Protein Chem. 60*, 271−340.
3. Dennison, C. (2005) Investigating the structure and function of cupredoxins, *Coord. Chem. Rev. 249*, 3025−3054.
4. Koch, M., Velarde, M., Harrison, M. D., Echt, S., Fischer, M., Messerschmidt, A., and Dennison, C. (2005) Crystal structures of oxidised and reduced stellacyanin from horseradish roots, *J. Am. Chem. Soc. 127*, 158−166.
5. Kim, S., Mollet, J. C., Dong, J., Zhang K., Park, S. Y., and Lord, E. M. (2003) Chemocyanin, a small basic protein from the lily stigma, induces pollen tube chemotropism, *Proc. Natl. Acad. Sci. U.S.A. 100*, 16125−16130.
6. Piontek, K., Antorini, M., and Choinowski, T. (2002) Crystal structure of a laccase from the fungus *Trametes versicolor* at 1.90 Å resolution containing a full complement of coppers, *J. Biol. Chem. 277*, 37663−37669.
7. Zaitseva, I., Zaitseva, V., Card, G., Moshkov, K., Bax, B., Ralph, A., and Lindley, P. (1996) The X-ray structure of human serum ceruloplasmin at 3.1 Å: Nature of the copper centres, *J. Biol. Inorg. Chem. 1*, 15−23.
8. Taylor, A. B., Stoj, C. S., Ziegler, L., Kosman, D. J., and Hart, P. J. (2005) The copper−iron connection in biology: Structure of the metallo-oxidase Fet3p, *Proc. Natl. Acad. Sci. U.S.A. 102*, 15459−15464.
9. Baker, E. N. (1988) Structure of azurin from *Alcaligenes denitrificans*. Refinement at 1.8 Å resolution and comparison of the two crystallographically independent molecules, *J. Mol. Biol. 203*, 1071−1095.
10. Nar, H., Messerschmidt, A., Huber, R., van de Kamp, M., and Canters, G. W. (1991) X-ray crystal structure of the two site-specific mutants His35Gln and His35Leu of Azurin from *Pseudomonas aeruginosa*, *J. Mol. Biol. 218*, 427−447.
11. Crane, B. R., Di Bilio A. J., Winkler, J. R., and Gray, H. B. (2001) Electron tunnelling in single crystals of *Pseudomonas aeruginosa* azurins, *J. Am. Chem. Soc. 123*, 11623−11631.
12. Kolczak, U., Dennison, C., Messerschmidt, A., and Canters, G. W. (2001) Azurin and azurin mutants, in *Handbook of Metalloproteins* (Messerschmidt, A., Huber, R., Poulos, T., and Wieghardt, K., Eds.) pp 1170−1194, John Wiley and Sons, Chichester, U.K.
13. Karlsson, B. G., Nordling, M., Pascher, T., Tsai, L. C., Sjölin, L., and Lundberg, L. G. (1991) Cassette mutagenesis of Met121 in azurin from *Pseudomonas aeruginosa*, *Protein Eng. 4*, 343−349.
14. den Blaauwen, T., van de Kamp, M., and Canters, G. W. (1991) Type 1 and 2 copper sites obtained by external addition of ligands to a His117Gly azurin mutant, *J. Am. Chem. Soc. 113*, 5050−5052.
15. Mizoguchi, T. J., Di Bilio, A. J., Gray, H. B., and Richards, J. H. (1992) Blue to type 2 binding. Copper(II) and cobalt(II) derivatives of a Cys112Asp mutant of *Pseudomonas aeruginosa* azurin, *J. Am. Chem. Soc. 114*, 10076−10078.
16. Romero, A., Hoitink, C. W. G., Nar, H., Huber, R., Messerschmidt, A., and Canters, G. W. (1993) X-ray analysis and spectroscopic characterization of M121Q azurin, *J. Mol. Biol. 229*, 1007−1021.
17. Messerschmidt, A., Prade, L., Kroes, S. J., Sanders-Loehr, J., Huber, R., and Canters, G. W. (1998) Rack-induced metal binding vs. flexibility: Met121His azurin crystal structures at different pH, *Proc. Natl. Acad. Sci. U.S.A. 95*, 3443−3448.
18. Gray, H. B., Malmström, B. G., and Williams, R. J. P. (2000) Copper coordination in blue proteins, *J. Biol. Inorg. Chem. 5*, 551−559.
19. Bertini, I., Ciurli, S., Dikiy, A., Gasanov, R., Luchinat, C., Martini, G., and Safarov, N. (1999) High-field NMR studies of oxidised blue copper proteins: The case of spinach plastocyanin, *J. Am. Chem. Soc. 121*, 2037−2046.
20. Bertini, I., Fernández, C. O., Karlsson, B. G. Leckner, J., Luchinat, C., Malmström, B. G., Nersissian, A. M., Pieratelli, R., Shipp, E., Valentine, J. S., and Vila, A. J. (2000) Structural information through NMR hyperfine shifts in blue copper proteins, *J. Am. Chem. Soc. 122*, 3701−3707.
21. Jaszewski, A. R., and Jezierska, J. (2001) Hybrid density functional approach to the isotropic and anisotropic hyperfine couplings with ^{14}N and ^{1}H nuclei in the blue copper proteins, *Chem. Phys. Lett. 343*, 571−580.
22. van Gastel, M., Nagano, Y., Zondervan, R., Canters, G. W., Jeuken, L. J. C., Warmerdam, G. C. M., de Waal, E. C., and Groenen, E. J. J. (2002) Hydrogen bonding in the blue-copper site. Resonance Raman study, *J. Phys. Chem. 106*, 4018−4021.
23. Musiani, F., Carloni, P., and Ciurli, S. (2004) The Asn38−Cys84 H-bond in plastocyanin, *J. Phys. Chem. 108*, 7495−7499.
24. Langen, R., Jensen, G. M., Jacob, U., Stephens, P. J., and Warshel, A. (1992) Protein control of iron−sulfur cluster redox potentials, *J. Biol. Chem. 267*, 25625−25627.
25. Dong, S., Ybe, J. A., Hecht, M. H., and Spiro, T. G. (1999) H-bonding maintains the active site of type 1 copper proteins: Site-directed mutagenesis of Asn38 in poplar plastocyanin, *Biochemistry 38*, 3379−3385.
26. Guss, J. M., and Freeman, H. C. (1983) Structure of oxidized poplar plastocyanin at 1.6 Å resolution, *J. Mol. Biol. 169*, 521−563.
27. Inoue, T., Nishio, N., Suzuki, S., Kataoka, K., Kohzuma, T., and Kai, Y. (1999) Crystal structure determinations of oxidized and reduced pseudoazurins from *Achromobacter cycloclastes*, *J. Biol. Chem. 274*, 17845−17852.
28. Cunane, L. M., Chen, Z., Durley, R. C. E., and Mathews, F. S. (1996) X-ray structure of the cupredoxin amicyanin, from *Paracoccus denitrificans*, refined at 1.31 Å resolution, *Acta Crystallogr., Sect. D: Biol. Crystallogr. 52*, 676−686.
29. Bond, C. S., Blankenship, R. E., Freeman, H. C., Guss, J. M., Maher, M. J., Selvaraj, F. M., Wilce, M. C. J., and Willingham, K. M. (2001) Crystal structure of auracyanin, a blue copper protein

from the green thermophilic photosynthetic bacterium *Chloroflexus aurantiacus*, *J. Mol. Biol. 306*, 47−67.
30. Nishiyama, M., Suzuki, J., Ohnuki, T., Chang, H. C., Horinouchi, S., Tutley, S., Adman, E. T., and Beppu, T. (1992) Site-directed mutagenesis of pseudoazurin from *Alcaligenes faecalis* S-6; Pro80Ala mutant exhibits marked increase in reduction potential, *Protein Eng. 5*, 177−184.
31. Libeu, C. A. P., Kukimoto, M., Nishiyama, M., Horinouchi, S., and Adman, E. T. (1997) Site-directed mutants of pseudoazurin: Explanation of increased redox potentials from X-ray structures and from calculation of redox potential differences, *Biochemistry 36*, 13160−13179.
32. Machczynski, M. C., Gray, H. B., and Richards, J. H. (2002) An outer-sphere hydrogen-bond network constrains copper coordination in blue proteins, *J. Inorg. Biochem. 88*, 375−380.
33. Carrell, C. J., Sun. D., Jiang, S., Davidson, V. L., and Mathews, F. S. (2004) Structural studies of two mutants of amicyanin from *Paracoccus denitrificans* that stabilize the reduced state of the copper, *Biochemistry 43*, 9372−9380.
34. Yanagisawa, S., and Dennison, C. (2004) Loop-contraction mutagenesis of type 1 copper sites, *J. Am. Chem. Soc. 126*, 15711−15719.
35. Li, C., Yanagisawa, S., Martins, B. M., Messerschmidt, A., Banfield M. J., and Dennison, C. (2006) Basic requirements for a metal binding site in a protein: The influence of loop shortening on the cupredoxin azurin, *Proc. Natl. Acad. Sci. U.S.A. 103*, 7258−7263.
36. Sato, K., Kohzuma, T., and Dennison, C. (2003) Active-site structure and electron-transfer reactivity of plastocyanins, *J. Am. Chem. Soc. 125*, 2101−2112.
37. Dennison, C., and Lawler, A. T. P. (2001) Investigation of the alkaline and acid transitions in umecyanin, a stellacyanin from horseradish roots, *Biochemistry 40*, 3158−3166.
38. Battistuzzi, G., Borsari, M., Canters, G. W., de Waal, E., Leonardi, A., Ranieri, A., and Sola, M. (2002) Thermodynamics of the acid transition in blue copper proteins, *Biochemistry 41*, 14293−14298.
39. Collaborative Computational Project, Number 4 (1994) *Acta Crystallogr., Sect. D: Biol. Crystallogr. 50*, 760−763.
40. Nar, H., Messerschmidt, A., Huber, R., van de Kamp, M., and Canters, G. W. (1991) Crystal structure analysis of oxidised *Pseudomonas aeruginosa* azurin at pH 5.5 and pH 9.0—A pH-induced conformational transition involves a peptide-bond flip, *J. Mol. Biol. 221*, 765−772.
41. Emsley, P., and Cowtan, K. (2004) Coot: Model-building tools for molecular graphics, *Acta Crystallogr., Sect. D: Biol. Crystallogr. 60*, 2126−2132.
42. Kleywegt, G. J., Zou, J. Y., Kjeldgaard, M., and Jones, T. A. (2001) in *International Tables for Crystallography: Crystallography of Biological Macromolecules* (Rossmann, M. G., and Arnold, E., Eds.) Vol. F, pp 353−356 and 366−367, Kluwer Academic Publishers, Dordrecht, The Netherlands.
43. Pascher, T., Karlsson, B. G., Nordling, M., Malmström, B. G., and Vänngård, T. (1993) Reduction potentials and their pH dependence in site-directed mutant forms of azurin from *Pseudomonas aeruginosa*, *Eur. J. Biochem. 212*, 289−296.
44. Kalverda, A. P., Salgado, J., Dennison, C., and Canters, G. W. (1996) Analysis of the paramagnetic copper(II) site of amicyanin by ^{1}H NMR spectroscopy, *Biochemistry 35*, 3085−3092.
45. Groeneveld, C. M., and Canters, G. W. (1985) The pH dependence of the electron self-exchange rate of azurin from *Pseudomonas aeruginosa* as studied by ^{1}H-NMR, *Eur. J. Biochem. 153*, 559−564.
46. Groeneveld, C. M., and Canters, G. W. (1988) NMR study of structure and electron-transfer mechanism of *Pseudomonas aeruginosa*, *J. Biol. Chem. 263*, 167−173.
47. Jeuken, L. J. C., van Vliet, P., Verbeet, M. P., Camba, R., McEvoy, J. P., Armstrong, F. A., and Canters, G. W. (2000) Role of the surface-exposed and copper-coordinating histidine in blue copper proteins: The electron-transfer and redox-coupled ligand binding properties of His117Gly azurin, *J. Am. Chem. Soc. 122*, 12186−12194.
48. Solomon, E. I., Szilagyi, R. K. George, S. D., and Basumallick, L. (2004) Electronic structures of metal sites in proteins and models: Contributions to function in blue copper proteins, *Chem. Rev. 104*, 419−458.
49. Sato, K., and Dennison, C. (2002) Effect of histidine 6 protonation on the active site structure and electron-transfer capabilities of pseudoazurin from *Achromobacter cycloclastes*, *Biochemistry 41*, 120−130.
50. Jeuken, L. J. C., Wisson, L. J., and Armstrong, F. A. (2002) The kinetics of a weakly electron-coupled proton transfer in azurin, *Inorg. Chim. Acta 331*, 216−223.
51. Tsai, L. C., Sjölin, L., Langer, V., Pascher, T., and Nar, H. (1995) Structure of the azurin mutant Phe114Ala from *Pseudomonas aeruginosa* at 2.6 Å resolution, *Acta Crystallogr., Sect. D: Biol. Crystallogr. 51*, 168−176.
52. DeLano, W. (2002) DeLano Scientific, San Carlos, CA.
53. van de Kamp, M., Floris, R., Hali, F. C., and Canters, G. W. (1990) Site-directed mutagenesis reveals that the hydrophobic patch of azurin mediates electron transfer, *J. Am. Chem. Soc. 112*, 907−908.
54. van Amsterdam, I. M. C., Ubbink, M., Einsle, O., Messerschmidt, A., Merli, A., Cavazzini, D., Rossi, G. L., and Canters, G. W. (2002) Dramatic modulation of electron transfer in protein complexes by crosslinking, *Nat. Struct. Biol. 9*, 48−52.
55. Li, H., Webb, S. P., Ivanic, J., and Jensen, J. H. (2004) Determinants of the relative reduction potentials of type 1 copper sites in proteins, *J. Am. Chem. Soc. 126*, 8010−8019.
56. Li, J., Nelson, M. R., Peng, C. Y., Bashford, D., and Noodleman, L. (1998) Incorporating protein environments in density functional theory: A self-consistent reaction field calculation of redox potentials of [2Fe2S] clusters in ferredoxin and phthalate dioxygenase reductase, *J. Phys. Chem. A 102*, 6311−6324.
57. Lin. I., Gebel, E. B., Machonkin, T. E., Westler, W. M., and Markley, J. L. (2005) Changes in hydrogen-bond strengths explain reduction potentials in 10 rubredoxin variants, *Proc. Natl. Acad. Sci. U.S.A. 102*, 14581−14586.
58. Guss, J. M., Harrowell, P. R., Murata, M., Norris, V. A., and Freeman, H. C. (1986) Crystal structures analyses of reduced (Cu^I) poplar plastocyanin at six pH values, *J. Mol. Biol. 192*, 361−387.
59. Vakoufari, E., Wilson, K. S., and Petratos, K. (1994) The crystal structures of reduced pseudoazurin from *Alcaligenes faecalis* S-6 at two pH values, *FEBS Lett. 347*, 203−206.
60. Zhu, Z., Cunane, L. M., Chen, Z. W., Durley, R. C. E., Mathews, F. S., and Davidson, V. L. (1998) Molecular basis for interprotein complex-dependent effects on the redox properties of amicyanin, *Biochemistry 37*, 17128−17136.
61. Buning, C., and Comba, P. (2000) Protonation of the copper(I) form of the blue copper proteins plastocyanin and amicyanin—A molecular dynamics study, *Eur. J. Inorg. Chem.* 1267−1273.
62. Guss, J. M., Merritt, E. A., Phizackerley, R. P., and Freeman, H. C. (1996) The structure of a phytocyanin, the basic blue protein from cucumber, refined at 1.8 Å resolution, *J. Mol. Biol. 262*, 686−705.
63. Canters, G. W., Kalverda, A. P., and Hoitink, C. W. G. (1993), in *The Chemistry of the Copper and Zinc Triads* (Welch, A. J., and Chapman, S. K., Eds.) pp 30−37, The Royal Society of Chemistry, Cambridge, U.K.
64. Dennison, C., Kohzuma, T., McFarlane, W., Suzuki, S., and Sykes, A. G. (1994) Reversible active site protonation and electron-transfer properties of *Achromobacter cycloclastes* pseudoazurin: Comparisons with other type 1 copper proteins, *Chem. Commun.* 581−582.
65. Buning, C., Canters, G. W., Comba, P., Dennison, C., Jeuken, L., Melter, M., and Sanders-Loehr, J. (2000) Loop-directed mutagenesis of the blue copper protein amicyanin from *Paracoccus versutus* and its effect on the structure and reactivity of the type 1 copper site, *J. Am. Chem. Soc. 122*, 204−211.
66. Dennison, C. (2005) Ligand and loop variations at type 1 copper sites: Influence on structure and reactivity, *Dalton Trans*. 3436−3442.
67. Battistuzzi, G., Borsari, M., Canters, G. W., di Rocco, G., de Waal, E., Arendsen, Y., Leonardi, A., Ranieri, A., and Sola, M. (2005) Ligand loop effects on the free energy change of redox and pH-dependent equilibria in cupredoxins probed on amicyanin variants, *Biochemistry 44*, 9944−9949.
68. Andrew, S. M., Thomasson, K. A., and Northrup, S. H. (1993) Simulation of electron-transfer self-exchange in cytochromes *c* and b_5, *J. Am. Chem. Soc. 115*, 5516−5521.

BI0606851